A Generalized Adsorption-Phase Transition Model to Describe Adsorption Rates in Flexible Metal Organic Framework RPM3-Zn

Angela D. Lueking,*[1,2] Cheng-Yu Wang,[1] Sarmishtha Sircar,[1] Christopher Malencia,[2] Hao Wang,[3] and Jing Li[3]

[1]Department of Energy & Mineral Engineering and EMS Energy Institute, [2]Department of Chemical Engineering, , The Pennsylvania State University, University Park, Pennsylvania 16802, USA

[3]Department of Chemistry and Chemical Biology, Rutgers University, Piscataway, NJ 08854, USA.

*Corresponding Author: 104 Materials Research Laboratory, adl11@psu.edu, 814-876-0005

Supporting Information

VI. Exploration of Catalysis Models

VII. Avrami-Type Analysis of the Rate Data

I. Supplemental Information

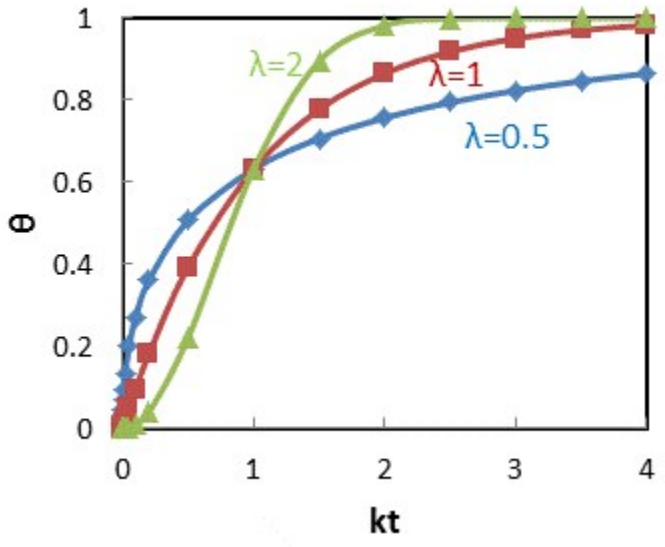

Figure S1. Effect of the l parameter on stretching ($\lambda<1$) or compressing ($\lambda>1$) about the convergence point (at kt=1).

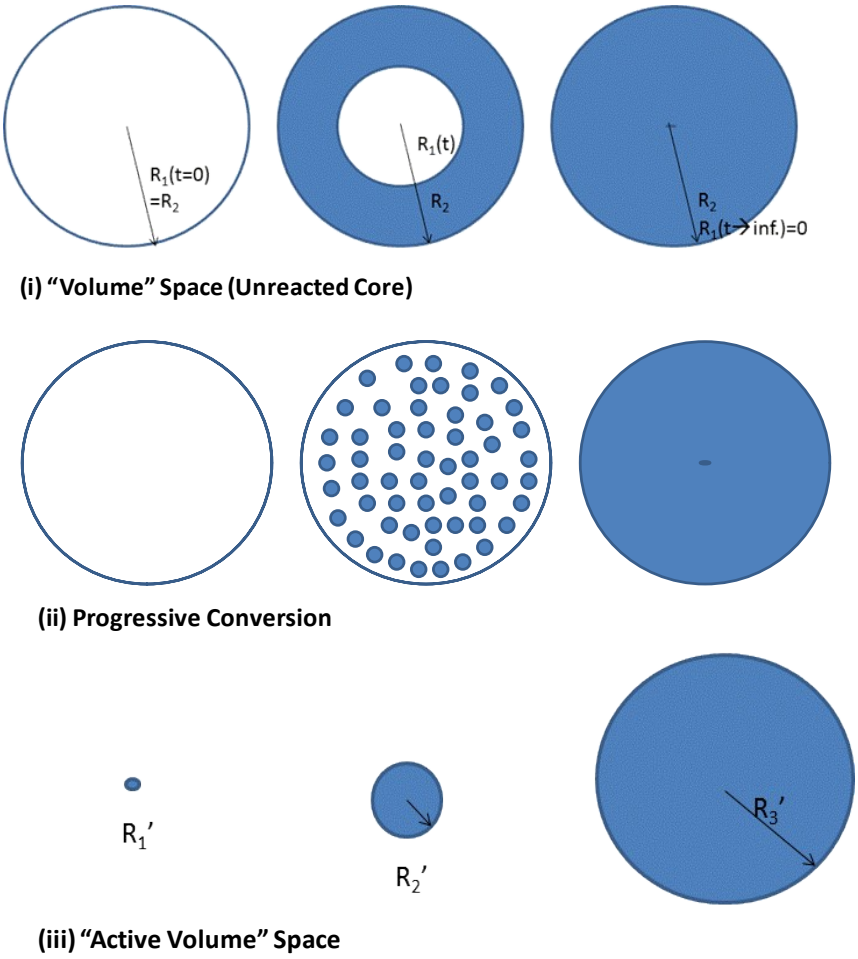

Figure S2: (i) Conceptualization of the unreacted core model: as gas diffuses into the particle with time, the inner unreacted core (white) shrinks as it is transformed to a product layer (blue). The particle is entirely unreacted at initial time (left) and completely transformed at infinite time (right). (ii) Homogenous diffusion into the particle and subsequent conversion via a progressive conversion mechanism typical in catalyst deactivation (iii) The 'effective volume' of the open phase in the GO procedure, which would include the summation of the blue regions. The volumes in (iii) are intended to be equivalent to those in (i), by appropriate adjustment of the radius.

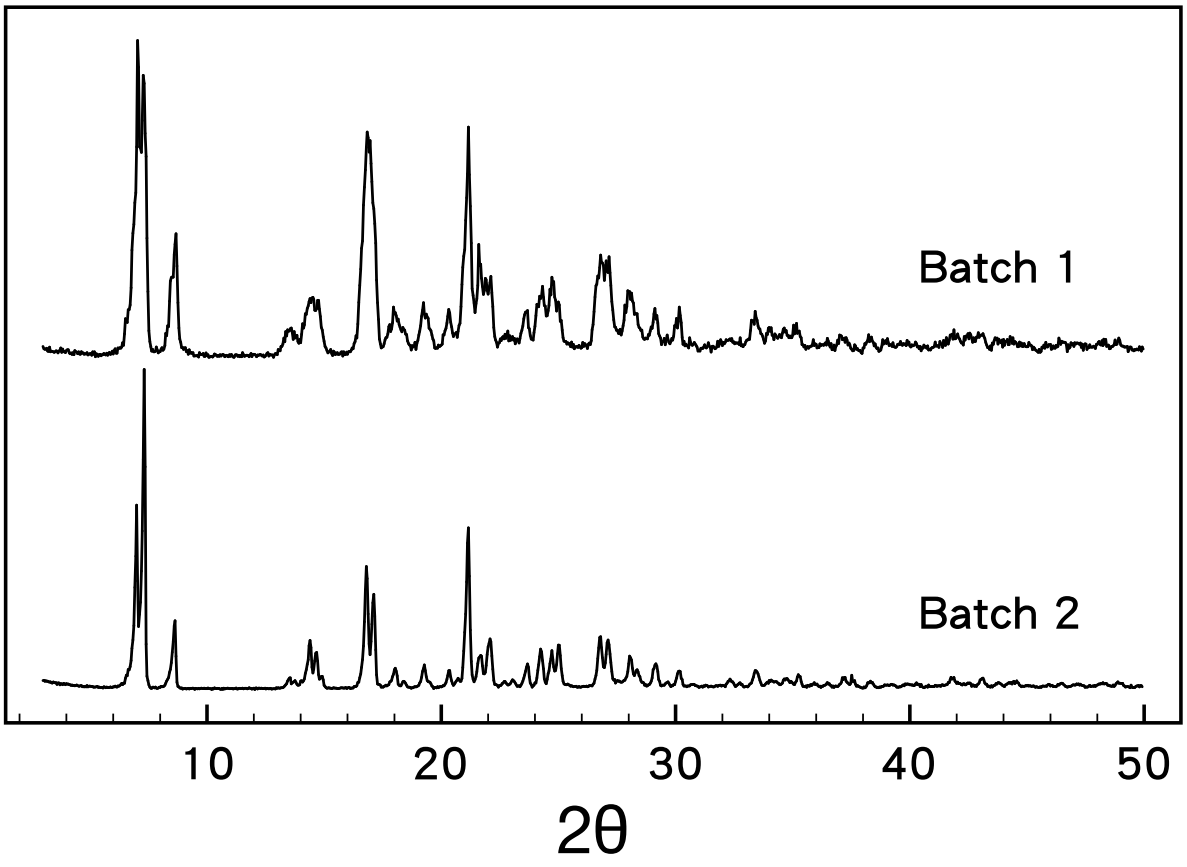

Figure S3: Powder X-Ray diffraction patterns of the two batches of RPM3-Zn samples studied in this work.

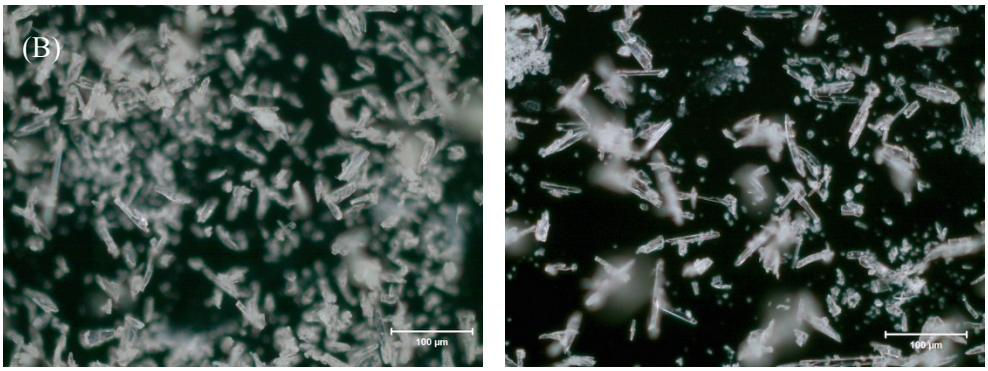

Figure S4: Optical microscopy of two batches (A: batch i; B: batch ii) of RPM3-Zn studied in this work. These are representative images of about 50 images that were taken with different magnifications to confirm the sizes and shapes. Both batches share the same rod-like shapes, with slight variations in length: 40-60 μm for Batch i and 50-70 μm for Batch ii.

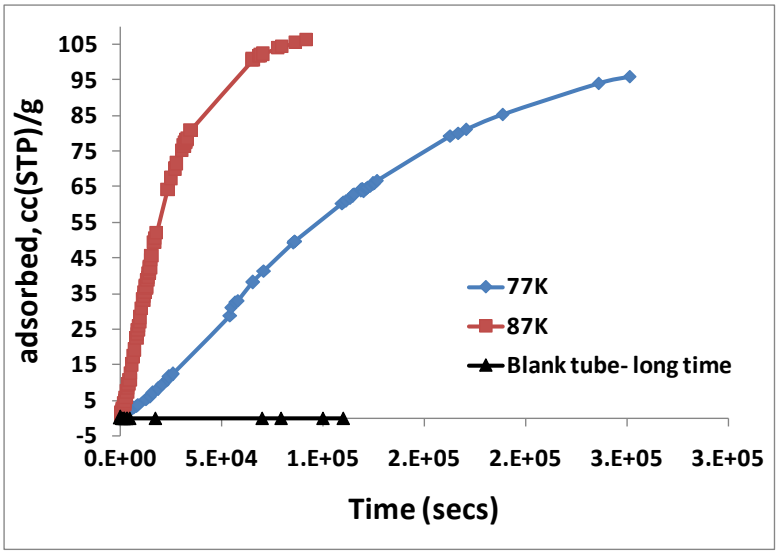

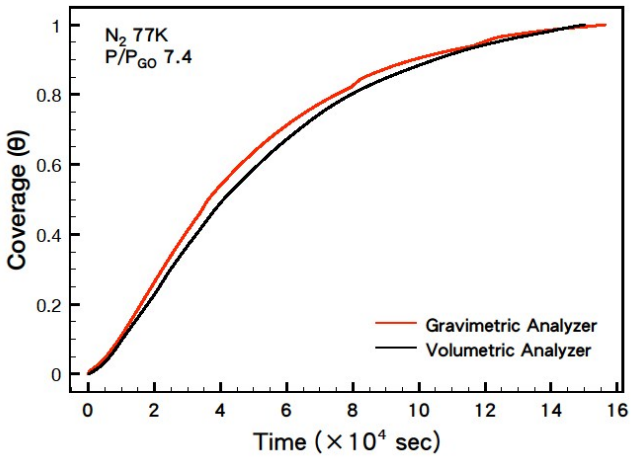

Figure S5. Validation of experimental methods. (a, top) Blank tube tests (black data) ensure uptake for extended time experiments cannot be attributed to leakage assuming a 100 mg sample mass, relative to the typical magnitude of the sample measurements (blue diamonds are the N_2 isotherm at 77K, P/Po=0.22 for Batch i; red squares are the Ar isotherm at 87K, P/Po = 0.15 for Batch i.) (b, bottom) Comparison of sequential adsorption isotherms measured on Batch ii at 77K and P/P_{GO}=7.4 (~230 mbar) on the volumetric and gravimetric equipment.

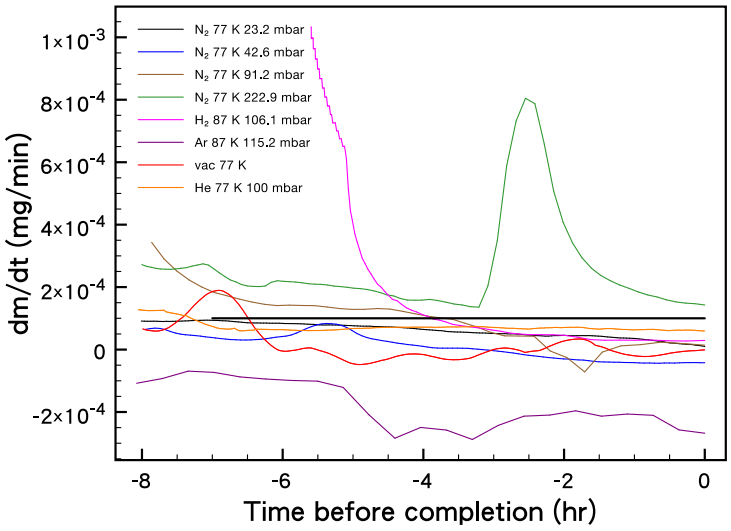

Figure S6: The sample weight derivative dm/dt in different environments (corresponding to the rate curves in the main paper) at 8 hours before the end of each kinetics curve. A spike in the green data is due to a refill of the liquid nitrogen temperature bath. The solid line is the criteria used as the equilibrium criteria from previous studies[1] and verified by a two blank experiments (vac 77K in red; He 77K 100 mbar in orange).

To assess the effect of various data handling parameters in fits of the rate curves, we selected a gas and adsorption conditions for which adsorption was very rapid, i.e. oxygen at 87 K 100 mbar. At these conditions, the uptake was quite rapid, with 10% of the uptake occurring during the 1 minute required to achieve the target pressure (i.e. 0.6 mmol/g after 1 minute versus final value of 5.6 mmol/g, Figure S7). The following data handling issues were considered: (1) unprocessed data to completion with truncated rate curve; (2) processing of (1) to remove spikes that occur during the initial valve opening; (3) removal of the ramping period where pressure is not constant; and (4) an extended equilibration time such that the rate curve was absolutely parallel to the x-axis. Comparing the obtained rate parameters for two select models (Table S1), shows the spike in the data due to valve opening has very little effect on the rate curves ('1' vs

'2', Table S1). Removal of the pressure ramping period leads to a ~1.5-fold difference in k of the LDF model and a ~1.05-fold difference in k of Gompertz model and a ~2-fold variation in the β parameter. Although not insignificant, these variations are relatively minor relative to variations seen between gases and conditions. Including a larger time scale leads to no variation in fitted parameters ('3' vs '4', Table S1). The latter point demonstrates the use of an 8-hour criteria for equilibration discussed above should have no large effect on curve fitting.

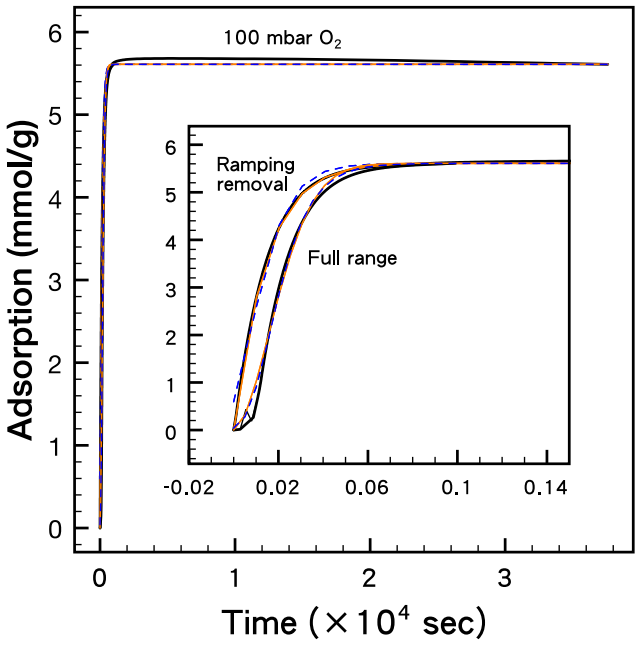

Figure S7: Curve fitting of SE model over oxygen 100 mbar adsorption kinetics with different selected time ranges and data processing. Curves labeled "Ramping Removal" consider the starting time to be the once the pressure goal is obtained, whereas "full range" considers the starting time to be the initiation of the pressure step (Model fits include: LDF: orange, Gompertz: blue dash line)

Table S1. The fitting parameters with different selected ranges

Case	Selected Range	Model	Fitted Constants (sec^{-1})	R^2
1	Unprocessed data, short time (to 0.14 x 10^4 sec, i.e. inset to Fig. S7)	LDF	$k = 4.22\times10^{-3}$	0.9863
		Gompertz	$k = 9.82\times10^{-3}$ $\beta = 4.83\times10^{-2}$	0.9993
2	Removal of spikes (associated with valve opening/closing)	LDF	$k = 4.22\times10^{-3}$	0.9863
		Gompertz	$k = 9.83\times10^{-3}$ $\beta = 4.83\times10^{-2}$	0.9993
3	Shift of starting time to remove the period where P was increasing (to 0.1×10^4 sec, i.e. inset to Fig. S7)	LDF	$k = 6.91\times10^{-3}$	0.9999
		Gompertz	$k = 1.05\times10^{-2}$ $\beta = 2.36\times10^{-2}$	0.9983
4	Shift of starting time to remove the period where P was increasing; Extended time range (to 4×10^4 sec; Fig. S7)	LDF	$k = 6.91\times10^{-3}$	0.9999
		Gompertz	$k = 1.05\times10^{-2}$ $\beta = 2.36\times10^{-2}$	0.9986

Conclusion: The extent of the plateau at long time did not effect fitted rate parameters (3 vs. 4). Truncating the initial time period where pressure is not constant may have a minor effect when adsorption is rapid.

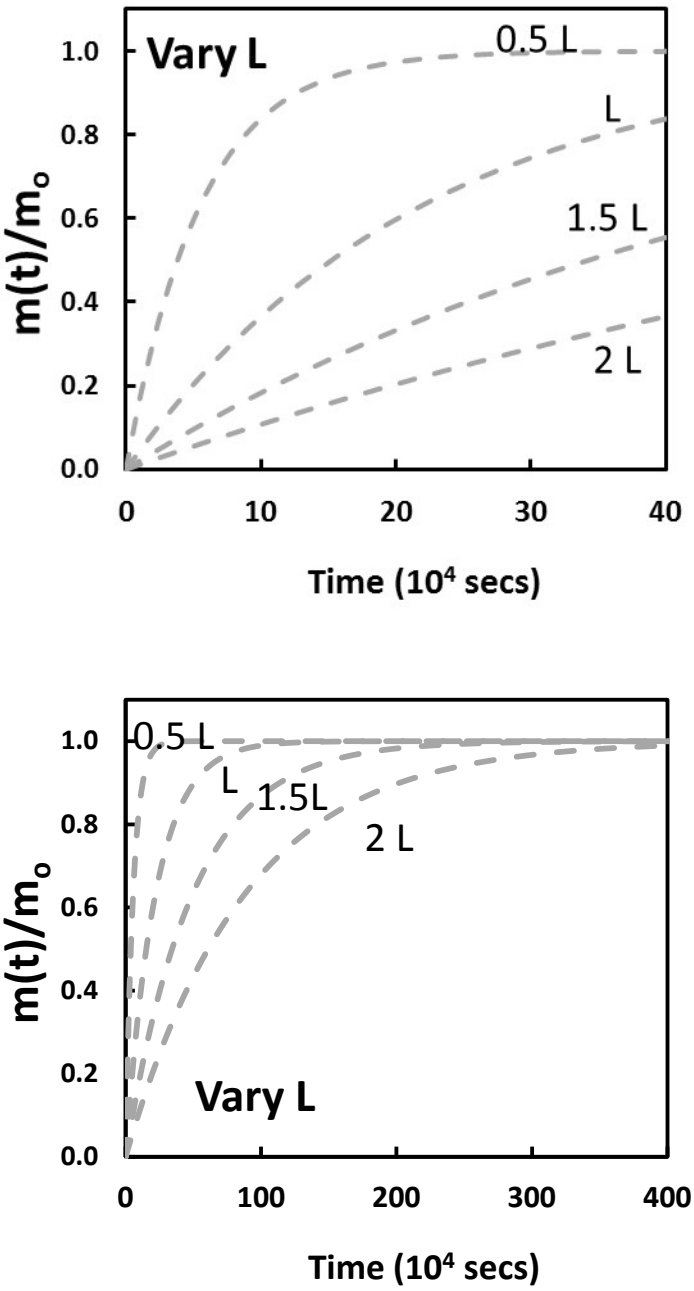

Figure S8: Effect of diffusion length (L) on the adsorption rate for the LDF model. The treatment assumes a constant diffusion coefficient ($1x10^{-9}$ cm^2/s) then varies L (base case is 150 μm) to determine whether the LDF model may significantly change shape. The same data is plotted on two different scales. Sigmoidal adsorption rates are not observed.

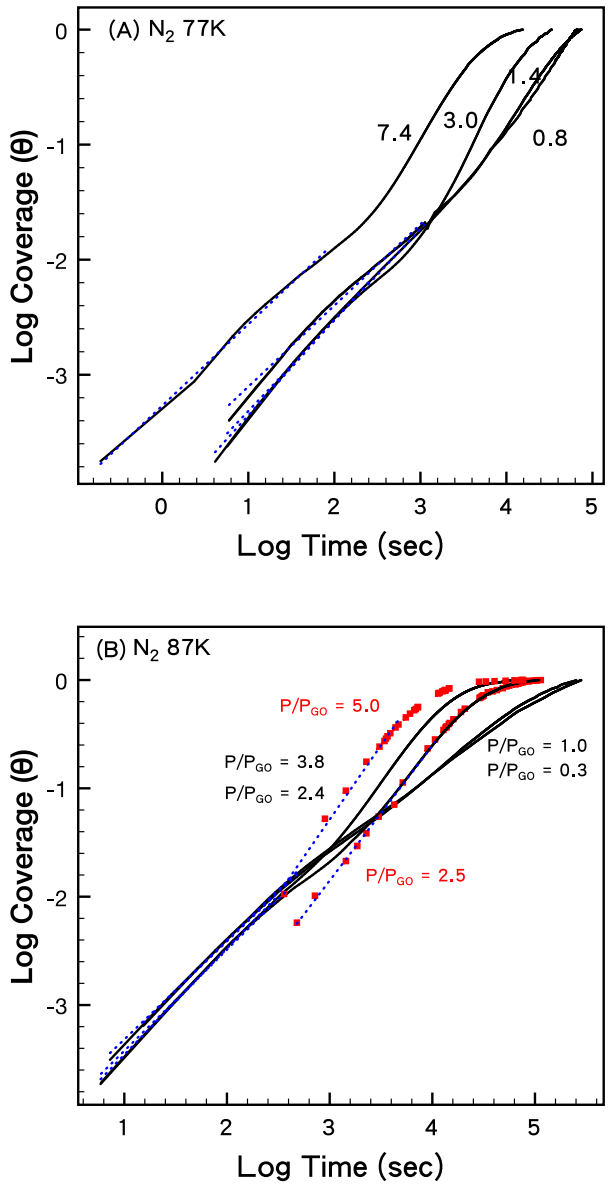

Figure S9: Fit of the N_2 rate data to the power law expression ($\theta=kt^n$) to ascertain the diffusion regime. If n=0.5, this is typically associated with Fickian diffusion, 0.5 < n < 1 is anomalous diffusion, n=1 is "Case II", and n>1 is "Super Case II". The slopes for the data at initial time (blue dotted lines) are 0.7-0.8 at 77K and 0.9-1.0 at 87 K*.

*Specifically: (A) 0.71, 0.79, 0.83, and 0.71 for P/P_{GO} 0.8, 1.4, 3.0, and 7.4; (B) 0.93, 0.91, 0.93, and 0.98 for P/P_{GO} 0.3, 1.0, 2.4, 3.8, respectively. The batch (i) volumetric data was also fit, but there was also much less short time data due to the nature of the manual volumetric collection.

II. Validation of Avrami's theory applied to adsorption (derivation)

A validation of Avrami's theory is to demonstrate that adsorption to a rigid host is consistent with Avrami's development. Notably, in the adsorption regime, data is commonly fit to the LDF and/or SE much more frequently than the MPD and more complex Fickian-based models. Generation of rate data via the MPD data leads to a curve that will have a shape parameter of 0.65.[2] Data that fits the LDF model with a shape parameter of 1 is generally attributed to activated diffusion through a surface potential.

To consider adsorption in a porous media to a rigid host, the phase transition is considered to be a transition from the "empty" pore to a pore that is filled with a condensed film. Thus the phase transition of interest is condensation of the gas to create an adsorbed film.

Similar to the MPD development, we presume diffusion occurs into a homogenous spherical particle, with an effective diffusivity that would take into account tortuosity and with the primary diffusion occurring in the pores. The geometry of the phase growth of adsorption is in the opposite direction as that generally considered in the Avrami development, i.e. the phase is growing from the outside diameter inwards such that the new phase is a growing annulus at the periphery of the sphere.

As this form generally arises in solutions to Fick's law[3], we first presume the distance penetrated by diffusion can be given by:

$$t=L^2/D \qquad \text{(S1)}$$

Then:

$$\frac{dL}{d(t^{0.5})} = D^{0.5} \qquad \text{(S2)}$$

For a single sphere, the volume of the outer annulus ('oa)' is given by

$$v_{oa} = \frac{4}{3}\pi\left[R^3 - r^3\right] \qquad \text{(S3)}$$

Where R is the outer volume of the sphere and r is the retreating interface of the inner core in which condensation/adsorption has not yet occurred, such that R=L+r. Then, the fractional volume of the outer annulus for the growing adsorbed phase in this region is:

$$\theta_{V1} = 1 - \left(1 - \frac{L(t)}{R}\right)^3 = \qquad \text{(S4)}$$

For $L=(tD)^{0.5}<R$. Defining $k = D/R^2$ requires that $t<k^{-0.5}=\tau_{max}$.

Following Avrami's development, we allow for an induction period:

$$L(t) = \frac{dL}{d\left(t^{0.5}\right)}(t-\tau)^{0.5} = D^{0.5}(t-\tau)^{0.5} \qquad \text{(S5)}$$

Then:

$$\theta_{V1} = 1 - \left(1 - \frac{D^{0.5}(t-\tau)^{0.5}}{R}\right)^3 = 1 - \left(1 - k^{0.5}(t-\tau)^{0.5}\right)^3 \qquad \text{(for } t< \tau_{max}\text{) (S6)}$$

Following the Avrami development, if there are a number of growing regions within the larger system, then the total system volume converted is given by:

$$\theta_V = \int_{\tau=0}^{t<\tau max} \dot{N}'\theta_{V1}d\tau = \int_{\tau=0}^{t<\tau max} \dot{N}'\left[1 - \left(1 - k^{0.5}(t-\tau)^{0.5}\right)^3\right]d\tau \qquad \text{(S7)}$$

Where $\dot{N}'$ is the rate of nucleation of the growing regions, in units of #/time/volume, given by[4]:

$$\frac{dN'}{dt} = \dot{N}' = pN \qquad \text{(S8)}$$

Where p is the probability of transformation, and N is the number of germ nuclei sites.

For consideration of a single homogenous spherical particle, there is a single growth region and the nucleation rate goes to zero:

$$\theta_{V1} = 1 - \left(1 - k^{0.5}t^{0.5}\right)^3 = k^{1.5}t^{1.5} - 3kt + 3k^{0.5}t^{0.5} \qquad \text{(S9)}$$

Which has the general form:

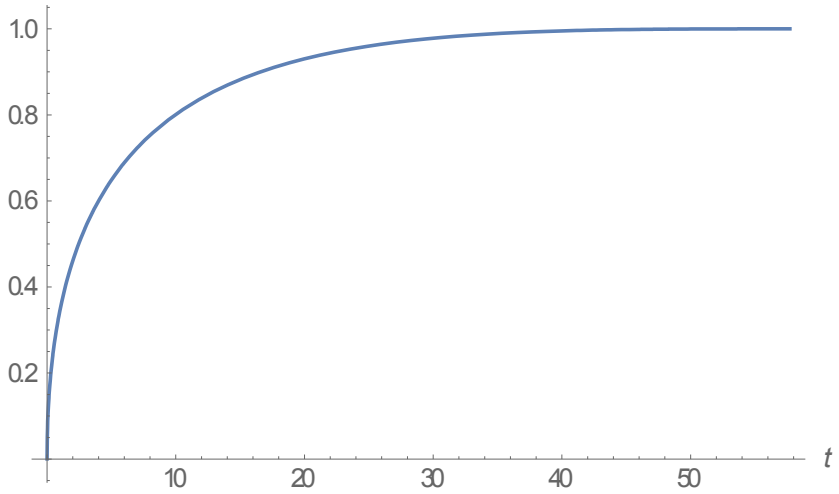

If the growth rate is linear:

$$\theta_{V1} = 1 - \left(1 - \frac{G(t-\tau)}{R}\right)^3 = 1 - \left(1 - k'(t-\tau)\right)^3 \qquad \text{(for } t < \tau_{max} = 1/k') \qquad \text{(S10)}$$

To convert these equations to the SE/CE function to develop an "apparent stretching parameter:

Determining slope analytically, for general SE

$$\theta_{V1} = 1 - e^{-(kt)^n}$$

$$1 - \theta_{V1} = e^{-(kt)^n}$$

$$-Ln(1 - \theta_{V1}) = (kt)^n$$

$$y = Ln(-Ln(1 - \theta_{V1})) = nLn(kt)$$

$$x = \ln(t)$$

$$t = e^x$$

$$y = nLn(k) + nLn(t) = nLn(k) + nx$$

$$\frac{dy}{dx} = n$$

For (S9):

$$1 - \theta_{V1} = \left(1 - k^{0.5}t^{0.5}\right)^3$$

$$-Ln(1 - \theta_{V1}) = -3ln\left(1 - k^{0.5}t^{0.5}\right)$$

$$y = Ln[-Ln(1 - \theta_{V1})] = Ln[-3ln\left(1 - k^{0.5}t^{0.5}\right)]$$

$$x = \ln(t)$$

$$t = e^x$$

$$y = Ln[-Ln(1 - \theta_{V1})] = Ln[-3ln\left(1 - k^{0.5}e^{x/2}\right)]$$

$$\frac{dy}{dx}$$

$$= \frac{1}{-3ln\left(1 - k^{0.5}e^{\frac{x}{2}}\right)} D_x\left(-3ln\left(1 - k^{0.5}e^{\frac{x}{2}}\right)\right) = \frac{1}{\left(1 - k^{0.5}e^{\frac{x}{2}}\right)ln\left(1 - k^{0.5}e^{\frac{x}{2}}\right)} D$$

Let u=$k^{0.5}e^{\frac{x}{2}}=k^{0.5}t^{0.5}$

$$\frac{dy}{dx}=-\frac{-\frac{1}{2}u}{(1-u)*Ln(1-u)}\sim\frac{1}{2}\frac{-u}{(1-u)*-u}\sim\frac{1}{2}$$

Where the latter approximation is valid for small u.

For (S10):

$$1-\theta_{V1}=(1-k't)^3$$

$$-Ln(1-\theta_{V1})=-3Ln(1-k't)$$

$$y=Ln[-Ln(1-\theta_{V1})]=Ln[-3Ln(1-k't)]=Ln[-3Ln(1-k'e^x)]$$

$$\frac{dy}{dx}=\frac{1}{-3Ln(1-k'e^x)}D_x(-3Ln(1-k'e^x))=\frac{1}{(1-k'e^x)Ln(1-k'e^x)}D_x(1-k$$

Let u=$k'e^x$*'*=*k't*

$$\frac{dy}{dx}=\frac{-u}{(1-u)*ln(1-u)}\sim\frac{-u}{(1-u)*-u}\sim1$$

Where the latter approximations are valid for small u.

To account for overlap, Avrami arrived at:

$$\theta_V=1-Exp[-\theta_{V,t\to0}] \qquad \text{(S11)}$$

Leading to:

$$\theta_{VD}=1-Exp[-k^{1.5}t^{1.5}+3kt-3k^{0.5}t^{0.5}] \quad \text{(S12)}$$

$$\theta_{VL}=1-Exp[-(k't)^3+3(k't)^2-3k't] \quad \text{(S13)}$$

Which would be approximated with:

$$\theta_{VD} \sim 1 - Exp\left[- \theta_{V,t \to 0} \right] \sim 1 - Exp\left[- k^{1.5} t^{1.5} \right] \quad \text{(S14)}$$

$$\theta_{VL} \sim 1 - Exp\left[- (k^{'} t)^{3} \right] \quad \text{(S15)}$$

RPM3-Zn exhibits rod-shaped crystals. In cylindrical coordinates, Equation S3 becomes:

$$v_{oac} = 4\pi\left[R^2 - r^2\right]Z \qquad \text{(S3')}$$

Where Z is the length of the cylinder, and it is assumed Z>>R so that edge effects may be neglected. The fractional volume in cylindrical coordinates is:

$$\theta_{V1c} = 1 - \left(\frac{R - L(t)}{R}\right)^2 \qquad \text{(S4')}$$

Substituting in S5 (which remains the same in cylindrical coordinates) and defining $k = D/R^2$ leads to:

$$\theta_{V1c} = 1 - \left(\frac{R - D^{0.5}(t-\tau)^{0.5}}{R}\right)^2 = 1 - \left(1 - k^{0.5}(t-\tau)^{0.5}\right)^2 \qquad \text{(for } t < \tau_{max}\text{)} \quad \text{(S6')}$$

Total system volume in cylindrical coordinates is given by:

$$\theta_{Vc} = \int_{\tau=0}^{t<\tau max} \dot{N}'\theta_{V1c}d\tau = \int_{\tau=0}^{t<\tau max} \dot{N}'\left[1 - \left(1 - k^{0.5}(t-\tau)^{0.5}\right)^2\right]d\tau \qquad \text{(S7')}$$

For consideration of a single cylinder, with no nucleation time:

$$\theta_{V1c} = 1 - \left(1 - (kt)^{0.5}\right)^2 = (kt)^{0.5} - kt \qquad \text{(S9')}$$

If linear growth rate had been assumed instead:

$$\theta_{V1c} = 1 - \left(\frac{R - G(t-\tau)}{R}\right)^2 = 1 - (1 - k'(t-\tau))^2 \qquad \text{(S10')}$$

A single cylinder will have no induction period with probability of 1 of inducing phase growth, leading to:

$$\theta_{V1C} = 1 - \left(1 - k't\right)^2 = 2k't - \left(k't\right)^2 \qquad \text{(S10')}$$

To convert these equations to the SE/CE function to develop an "apparent stretching parameter:

First, cylindrical case, sqrt t growth, i.e. *For (S9')*:

$$1 - \theta_{V1c} = \left(1 - (kt)^{0.5}\right)^2$$

$$-Ln(1-\theta_{V1c}) = -2ln\left(1-k^{0.5}t^{0.5}\right)$$

$$y = Ln[-Ln(1-\theta_{V1})] = Ln[-2ln\left(1-k^{0.5}t^{0.5}\right)]$$

$$x = \ln(t)$$

$$t = e^{x}$$

Let $u = k^{0.5}e^{\frac{x}{2}}$

$du = 0.5k^{0.5}e^{\frac{x}{2}}dx = 0.5u\,du$

$$y = Ln[-2ln(1-u)]$$

$$\frac{dy}{dx} = \frac{udy}{2du} = \frac{-u}{2(1-u)ln(1-u)} \sim \frac{1}{2}\frac{-u}{2(1-u)*-u} \sim \frac{1}{2}$$

Where the latter approximation is valid for small u.

<u>*For the cylindrical case, dL/dt is linear, i.e. for (S10'):*</u>

$$y = Ln[-Ln(1-\theta_{V1})] = Ln\left[-Ln\left[\left(1-k't\right)^2\right]\right] = Ln\left[-Ln\left[(1-u)^2\right]\right]$$

Let $u = k't = ke^{x}$

$du = k'e^{x}dx = udx$

$$\frac{dy}{dx} = u\frac{dy}{du} = u\frac{-2(1-u)}{(1-u)^2Ln\left[(1-u)^2\right]} = \frac{-u}{(1-u)Ln[(1-u)]} \sim \frac{-u}{(1-u)(-u)} \sim 1$$

Where the latter approximation is valid for small u.

$$1 - \theta_{V1c} = (1 - k't)^2$$

$$y = Ln[- Ln(1 - \theta_{V1}) =$$

III. Derivation of Gompertz Tumor Growth Model

The Gompertz model is applied to tumor growth rates. We consider growth of the *effective cumulative volume* (See Figure S2) of the open phase to be analogous to the growth of a tumor, in that it is growing under constrained conditions. For tumors, the rate of exponential growth decreases as the surface area to volume ratio of the tumor limits nutrient supply to the bulk of the tumor.[3] Mathematically:

$$\frac{dV}{dt} = r(t)V \qquad \text{(SIII-1)}$$

Where V represents the volume of the tumor and $r(t)$ is the time-dependent rate of tumor growth. The rate is assumed to decrease with time according to a first order rate expression:

$$\frac{dr}{dt} = -kr \qquad \text{(SIII-2)}$$

Leading to:

$$V = V_O e^{-\frac{r_O}{k}e^{-kt}} \quad \text{(SIII-3)}$$

The final mathematical form of the Gompertz function is thus a decaying exponential, with a limiting final size, V_O. The treatment of the rate $r(t)$ as an exponential decay appears to be an assumed/empirical treatment of the process, justified based on a decreasing surface area to volume ratio,[3,4] as we have found no theoretical justification of this treatment.

Reapplying this development to the GO phenomenon, we consider the effective volume of the open phase, V_o, which is the cumulative volume of the open phase at a given time, irrespective of whether the open to closed transformation occurs at a shrinking annular interface (as in the

unreacted core model) or geometrically dispersed throughout the particle (as in the progressive conversion model). The growth rate of the open phase depends upon the 'nutrients' provided by the conversion of the closed phase. The rate of increase in the open phase is dependent upon the availability of the nutrients, and thus the rate of growth is time-dependent:

$$\frac{dV_o}{dt} = r(t)V_o \qquad \text{(SIII-4)}$$

In the simplest case, the rate can be treated as proportional to the fraction of closed sites remaining:

$$r(t) = \frac{N_c(t)}{N_c^o}\beta = (1 - \frac{V_o(t)}{V_{o,\infty}})\beta = (1 - \theta_V)\beta \qquad \text{(SIII-5)}$$

Where β is the intrinsic rate of opening under non-limiting conditions, N_C is the number of closed sites at any time, and N_c^o is the initial number of closed sites. Relation of the fraction of closed sites to fractional volume conversion (θ_V) assumes only a constant dimension to relate number of sites to volume, without assuming a geometry in which the transformation occurs or conservation of volume between open and closed phase. If we assume that the net availability of the closed phase decays exponentially through the combined process of reaction and diffusion:

$$\frac{dN_c(t)}{dt} = -kN_c(t) \qquad \text{(SIII-6)}$$

Then, analogous to the development of the tumor growth model:

$$\Rightarrow r(t) = \beta e^{-kt} \qquad \text{(SIII-7)}$$

Where *k* is the rate at which this conversion decays with time, or equivalently, the net rate at which the closed phase converts to open phase through the combined process of reaction and diffusion.

At initial time, θ_V must not be equal to zero, as some seeds must exist for the conversion to begin. Thus, we use $\theta_V \rightarrow 1$ as $t \rightarrow \infty$ to solve the differential equation. Then the rate of conversion is β, according to (7). This leads to:

$$V_o(t) = V_{o,\infty} e^{-\frac{\beta}{k}e^{-kt}}$$
$$\Rightarrow \theta(t) = e^{-\frac{\beta}{k}e^{-kt}} = e^{-\alpha e^{-kt}} \qquad \text{(SIII-8)}$$

Where, in the final expression, the subscript on fractional volume conversion has been dropped due to the equivalency between mass and volume developed (see main paper, Equation 3), and $\theta(t)$ is simply the progress towards adsorptive equilibrium. As β is the intrinsic rate of transformation at initial time when there is no limit to the closed phase, and *k* is the rate constant which describes the conversion of closed phase to open phase (and thus is dependent upon both diffusion and reaction), the ratio of these two numbers ($\beta/k=\alpha$), is similar to the Deborah number, in that it is rate of reaction to rate of overall conversion. In this mathematical description, $\theta(0) \rightarrow e^{-\alpha}$ at initial time, as stated above, there must be some initial 'seeds' in this type of growth for conversion to begin. When β is large relative to *k*, $\theta(0) \rightarrow 0$, as expected. Mathematically, when β is small relative to *k*, $\theta(0) \rightarrow 1$. However, since *k* is the conversion rate and requires reaction to take place for conversion to occur, this scenario is unphysical.

IV. Full Data Fitting Results of RPM3-Zn adsorption rate data.

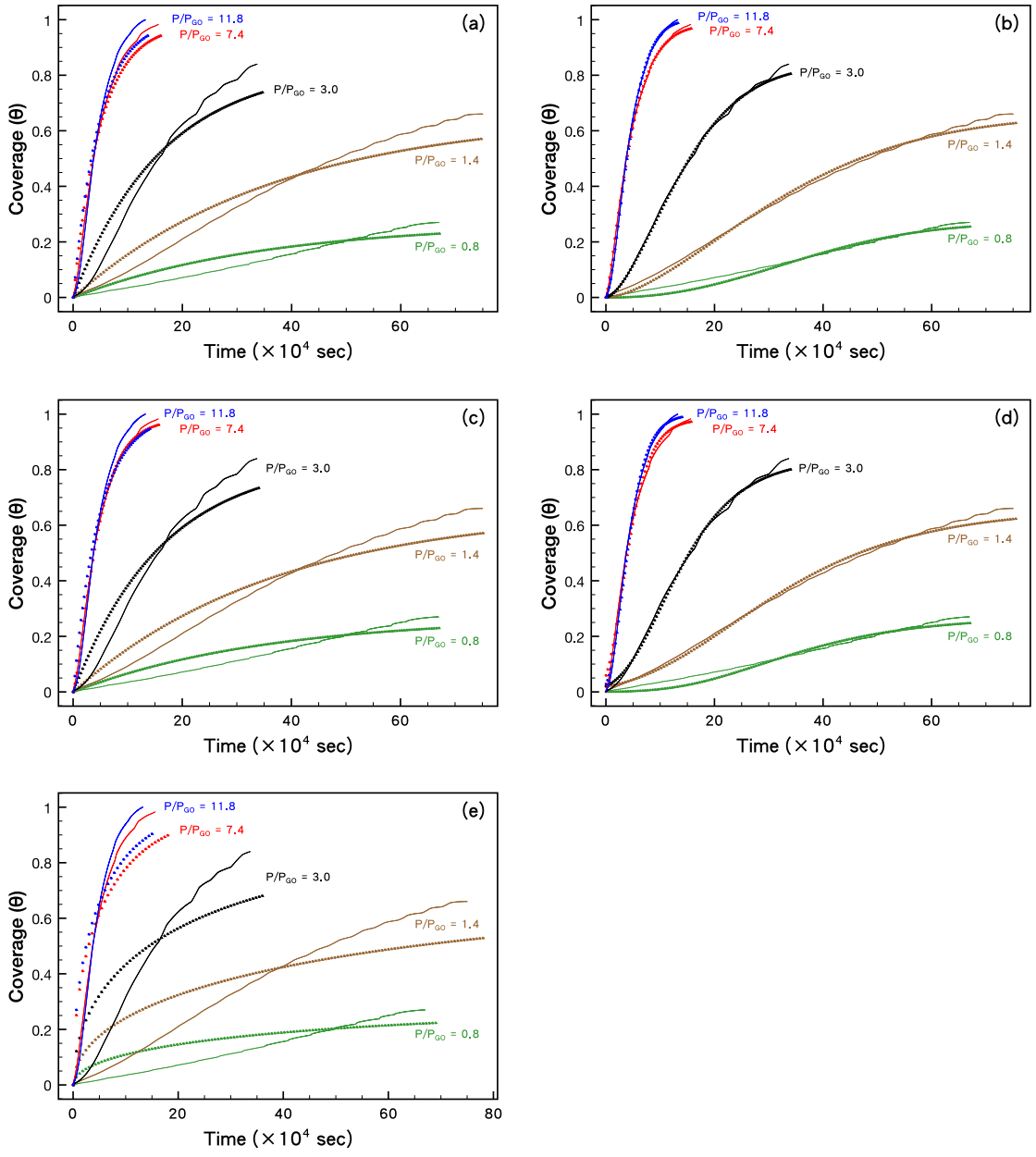

Figure S10: Fits of the 77K N_2 data to (a) DE, LDF, SE, (b) CE, (c) PD, (d) Gompertz, and (e) MPD. The fits to DE, LDF, and SE converged to the same values. The SE constrains the shape parameter to be <1, whereas the CE has no constraints on the shape parameter.

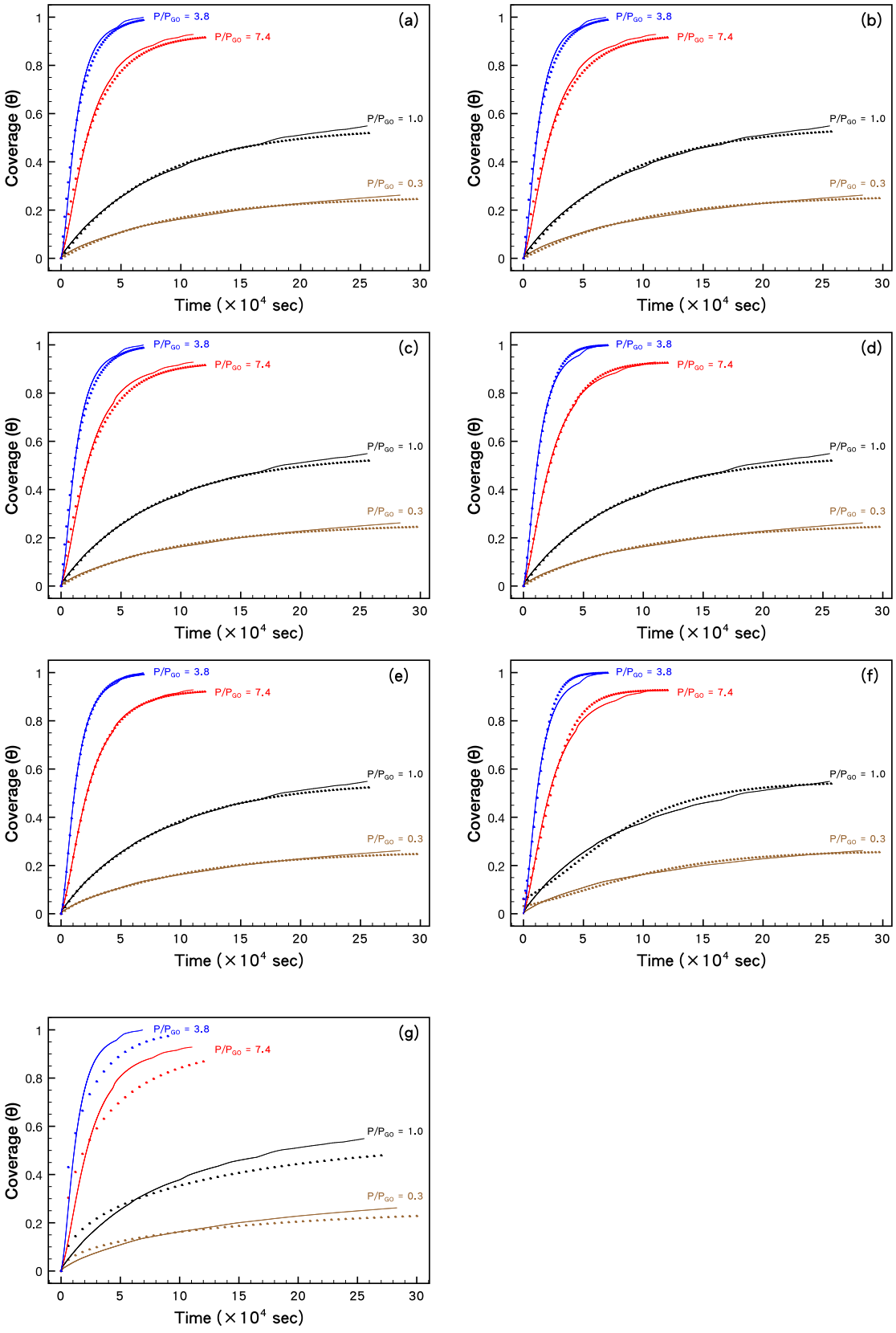
(a)
(b)
(c)
(d)
(e)
(f)
(g)
Coverage (θ)
Time (×10^4 sec)
P/P_GO = 3.8
P/P_GO = 7.4
P/P_GO = 1.0
P/P_GO = 0.3

Figure S11: Fits of the 87K N_2 data to (a) DE (b) LDF (c) SE (with λ constrained to be <1), (d) SE/CE (no constraints), (e) PD, (f) Gompertz, and (g) MPD. The fits to DE, LDF, and SE converged to the same values. The SE constrains the shape parameter to be <1, whereas the CE has no constraints on the shape parameter.

Table S2: Overview/Summary of fitting statistics to evaluate the 'best' model. (Top line is R^2; bottom line is AIC parameter.) Highlighted cell is the model with the best AIC parameter.

Sample Shorthand Notation (Gas(A=Ar; N=N_2; H=H_2) Temp(K)_P(mbar)P/P_{GO})	Common Adsorption Models				Reaction-diffusion		Growth Models	
	MPD	LDF	DE	SE ($\lambda \leq 1$ used as a constraint)	GO	PD	Gompertz	SE/CE (λ allowed to vary)
N77_23 0.8	0.9690 -2569	0.9837 -3939	0.9837 -3937	0.9837 -3937	0.9926 -5625	0.9837 -3935	0.9959 -6896	0.9976 -7974
N77_43 1.4	0.9432 -2509	0.9838 -5850	0.9838 -5848	0.9838 -5848	0.9976 -10888	0.9838 -5845	0.9986 -12382	0.9987 -12537
N77_220 1.6	0.8949 -26.3	0.9677 -73	0.9677 -72	0.9677 -71	0.9972 -167	0.9978 -177	0.9998 -269	0.9997 -255**
N77_91 3.0	0.9432 -1286	0.9844 -3030	0.9844 -3028	0.9844 -3027	0.9992 -6959	0.9830 -2907	0.9994 -7396	0.9997 -8405
A77_92	0.9166 -45	0.9695 -130	0.9695 -128	0.9695 -128	0.9952 -281	0.9683 -123	0.9991 -426	0.9996 -489
N77_223* 7.4	0.9691 -4920	0.9963 -11874	0.9963 -11872	0.9963 -11871	0.9999 -24012	0.9999 -23268	0.9986 -15030	0.9999 -23032**
N77_355* 12	0.9602 -1579	0.9904 -3670	0.9904 -3668	0.9904 -3668	0.9999 -10463	0.9904 -3667	0.9996 -8200	0.9999 -9858
N87_30 0.3	0.9843 -3221	0.9982 -6073	0.9984 -6217	0.9989 -6708***	0.9986 -6412	0.9994 -7482	0.9948 -4673	0.9989 -6708***
N87_106 1.0	0.9799 -6126	0.9994 -15163	0.9995 -15684	0.9997 -16913 ***	0.9996 -16178	0.9998 -18320	0.9946 -9582	0.9997 - 16913** *
N87_265 2.4	0.9703 -6075	0.9974 -15156	0.9974 -15154	0.9974 -15152	1.0000 -30382	1.0000 -34058	0.9980 -16128	0.9998 -25123
N87_414 2.5	0.9762 -76	0.9982 -196	0.9982 -194	0.9982 -194	0.9999 -313	0.9999 -319	0.9970 -171	0.9995 -256
N87_414 3.8	0.9722 -5277	0.9969 -12632	0.9969 -12630	0.9969 -12629	0.9999 -25987	1.0000 -29882	0.9982 -14386	0.9997 -20057
N87_829 5.0	0.9808 -63	0.9985 -155	0.9985 -153	0.9985 -152	0.9999 -261	0.9999 -267	0.9981 -144	0.9998 -226
A87_115 0.2	0.9763 -10945	0.9988 -28758	0.9988 -28756	0.9988 -28751	0.9999 -47409	1.0000 -51316	0.9978 -25074	0.9998 -40284
H87_106	0.9987 -496	0.9758 -192	0.9984 -471	0.9996 -603	0.9984 -469	0.9984 -467**	0.9804 -212	0.9996 -603

*Although the GO-Kinetic model had the best statistics for two cases (N77_355_12 and N87_30_0.3), this was not selected as the best model, as the denominator approached zero for the resulting fitted parameters and the PSSA was

invalidated (See **Table S3** (C)). Thus, the model with the second best fitting statistics is highlighted.
**These models had the second (or third) best fitting statistics in the highlighted cases, and are considered "best" after invalidation of the models with better statistics, for reasons discussed in the text.
***In these cases, the fitting statistics of the SE and CE are the same, as the resulting shape parameter when it was not constrained in any way was less than 1.

Table S3: The parameters corresponding to Figures S10-11.

(A) LDF

Sample Shorthand Notation (Gas(A=Ar; N=N_2; H=H_2) Temp(K)_P(mbar) $P/P_{GO)}$)	Fitted Rate Constant k (s^{-1})
N77_23 0.8	2.85×10^{-6}
N77_43 1.4	2.68×10^{-6}
N77_220 1.6	4.55×10^{-6}
N77_91 3.0	6.10×10^{-6}
A77_92	7.94×10^{-6}
N77_223 7.4	1.99×10^{-5}
N77_355 12	2.10×10^{-5}
N87_30 0.3	1.03×10^{-5}
N87_106 1.0	1.24×10^{-5}
N87_265 2.4	3.61×10^{-5}
N87_414 2.5	3.74×10^{-5}
N87_414 3.8	6.49×10^{-5}
N87_829 5.0	1.12×10^{-4}
A87_115 0.2	7.24×10^{-5}
H87_106	4.48×10^{-4}

(B) DE (A_1=A_2=0.5 assumed; Highlighted row had the best fitting statistics relative to the other models.)

Sample Shorthand Notation (Gas(A=Ar; N=N_2; H=H_2) Temp(K)_P(mbar) $P/P_{GO)}$)	Fitted Rate Constant k_1 (s^{-1})	Fitted Rate Constant k_2 (s^{-1})
N77_23 0.8	2.85×10^{-6}	2.85×10^{-6}
N77_43 1.4	2.68×10^{-6}	2.68×10^{-6}
N77_220 1.6	4.55×10^{-6}	4.55×10^{-6}
N77_91 3.0	6.10×10^{-6}	6.10×10^{-6}
A77_92	7.94×10^{-6}	7.94×10^{-6}
N77_223 7.4	1.99×10^{-5}	1.99×10^{-5}
N77_355 12	2.10×10^{-5}	2.10×10^{-5}
N87_30 0.3	7.53×10^{-6}	1.43×10^{-5}
N87_106 1.0	9.31×10^{-6}	1.64×10^{-5}
N87_265 2.4	3.61×10^{-5}	3.61×10^{-5}
N87_414 2.5	3.74×10^{-5}	3.74×10^{-5}
N87_414 3.8	6.49×10^{-5}	6.49×10^{-5}
N87_829 5.0	1.12×10^{-4}	1.12×10^{-4}
A87_115 0.2	7.24×10^{-5}	7.24×10^{-5}
H87_106	1.41×10^{-4}	1.77×10^{-3}

(C) GO-Kinetics (A_1=A_2=0.5 assumed. Red text denotes problems with the resulting best model/fitting parameters.)

Sample Shorthand Notation (Gas(A=Ar; N=N_2; H=H_2) Temp(K)_P(mbar) P/P_{GO}))	Fitted Rate Constant k_{GO} (s^{-1})	Fitted Rate Constant k_{d1} (s^{-1})	k_{GO}:k_{d1}	Fitted Rate Constant k_{d2} (s^{-1})
N77_23 0.8	5.59×10^{-6}	5.59×10^{-6}	1.00	5.59×10^{-6}
N77_43 1.4	5.80×10^{-6}	5.80×10^{-6}	1.00	5.80×10^{-6}
N77_220 1.6	1.07×10^{-5}	1.07×10^{-5}	1.00	1.07×10^{-5}
N77_91 3.0	1.33×10^{-5}	1.33×10^{-5}	1.00	1.33×10^{-5}
A77_92	1.74×10^{-5}	1.74×10^{-5}	1.00	1.74×10^{-5}
N77_223 7.4	3.09×10^{-5}	3.87×10^{-5}	0.80	2.41×10^{-4}
N77_355 12	4.43×10^{-5}	4.43×10^{-5}	1.00	4.43×10^{-5}
N87_30 0.3	2.29×10^{-5}	8.72×10^{-6}	2.63	5.00×10^{9}
N87_106 1.0	2.64×10^{-5}	1.09×10^{-5}	2.42	8.08×10^{9}
N87_265 2.4	4.43×10^{-5}	1.57×10^{-4}	0.28	7.55×10^{-4}
N87_414 2.5	8.96×10^{-5}	3.83×10^{-5}	2.34	2.51×10^{-4}
N87_414 3.8	7.95×10^{-5}	3.69×10^{-4}	0.22	5.73×10^{-4}
N87_829 5.0	1.34×10^{-4}	6.78×10^{-4}	0.20	2.20×10^{-3}
A87_115 0.2	8.25×10^{-5}	4.22×10^{-4}	0.20	9.76×10^{-3}
H87_106	4.11×10^{12}	1.41×10^{-4}	2×10^{16}	1.77×10^{-3}

(D) PD (Highlighted rows had the best fitting statistics relative to the other models.)

Sample Shorthand Notation (Gas(A=Ar; N=N_2; H=H_2) Temp(K)_P(mbar) P/P_{GO})	Fitted Rate Constant k_{GO} (s^{-1})	Fitted Rate Constant k_{d1} (s^{-1})	Fitted Rate Constant k_{d2} (s^{-1})
N77_23 0.8	4.56×10^{-4}	2.85×10^{-6}	2.28×10^{-6}
N77_43 1.4	7.97×10^{-4}	2.68×10^{-6}	4.49×10^{-5}
N77_220 1.6	1.07×10^{-5}	8.30×10^{-6}	2.38×10^{-8}
N77_91 3.0	1.35×10^{-3}	6.10×10^{-6}	1.26×10^{-3}
A77_92	2.43×10^{-3}	7.94×10^{-6}	2.67×10^{-3}
N77_223 7.4	3.15×10^{-5}	2.50×10^{-5}	8.12×10^{-6}
N77_355 12	1.03×10^{-3}	2.10×10^{-5}	1.41×10^{-5}
N87_30 0.3	4.35×10^{-5}	9.92×10^{-6}	1.69×10^{-5}
N87_106 1.0	5.24×10^{-5}	1.21×10^{-5}	1.65×10^{-5}
N87_265 2.4	8.98×10^{-5}	4.06×10^{-5}	1.35×10^{-5}
N87_414 2.5	3.46×10^{-5}	1.42×10^{-4}	5.98×10^{-6}
N87_414 3.8	1.79×10^{-4}	7.31×10^{-5}	1.31×10^{-5}
N87_829 5.0	3.59×10^{-4}	1.24×10^{-4}	3.58×10^{-5}
A87_115 0.2	3.96×10^{-5}	2.37×10^{-4}	3.81×10^{-5}
H87_106	4.58×10^{-4}	2.51×10^{-4}	9.79×10^{-4}

(E) Gompertz (Highlighted row had the best fitting statistics relative to the other models.)

Sample Shorthand Notation (Gas(A=Ar; N=N_2; H=H_2) Temp(K)_P(mbar) $P/P_{GO)}$)	Fitted Rate Constant k (s^{-1})	Fitted Rate Constant β (s^{-1})	$\alpha=\beta/k$ Pseudo-Deborah Number (see main text)
N77_23 0.8	6.41×10^{-6}	3.98×10^{-5}	6.2
N77_43 1.4	5.46×10^{-6}	1.93×10^{-5}	3.5
N77_220 1.6	1.16×10^{-5}	5.15×10^{-5}	4.4
N77_91 3.0	1.28×10^{-5}	4.77×10^{-5}	3.7
A77_92	1.93×10^{-5}	9.31×10^{-5}	4.8
N77_223 7.4	3.58×10^{-5}	1.00×10^{-4}	2.8
N77_355 12	4.19×10^{-5}	1.50×10^{-4}	3.6
N87_30 0.3	1.51×10^{-5}	3.17×10^{-5}	2.1
N87_106 1.0	1.90×10^{-5}	4.19×10^{-5}	2.2
N87_265 2.4	6.48×10^{-5}	1.76×10^{-4}	7.1
N87_414 2.5	6.92×10^{-5}	1.95×10^{-4}	2.8
N87_414 3.8	1.17×10^{-4}	3.24×10^{-4}	2.8
N87_829 5.0	2.00×10^{-4}	5.25×10^{-4}	2.6
A87_115 0.2	1.23×10^{-4}	3.08×10^{-4}	2.5
H87_106	4.54×10^{-4}	7.43×10^{-4}	1.6

(F) SE/CE (shape parameter, λ, was allowed to vary; Highlighted rows had the best fitting statistics relative to the other models.)

Sample Shorthand Notation (Gas(A=Ar; N=N_2; H=H_2) Temp(K)_P(mbar) P/P_{GO}))	Fitted Rate Constant k (s^{-1})	Other Fitted Parameter λ; λ allowed to vary
N77_23 0.8	2.40×10^{-6}	2.24
N77_43 1.4	2.67×10^{-6}	1.58
N77_220 1.6	5.07×10^{-6}	1.77
N77_91 3.0	6.11×10^{-6}	1.59
A77_92	8.07×10^{-6}	1.86
N77_223 7.4	1.99×10^{-5}	1.26
N77_355 12	2.03×10^{-5}	1.51
N87_30 0.3	1.02×10^{-5}	0.917
N87_106 1.0	1.22×10^{-5}	0.947
N87_265 2.4	3.66×10^{-5}	1.21
N87_414 2.5	3.78×10^{-5}	1.17
N87_414 3.8	6.52×10^{-5}	1.24
N87_829 5.0	1.15×10^{-4}	1.18
A87_115 0.2	7.31×10^{-5}	1.13
H87_106	3.92×10^{-4}	0.584

(G) SE (shape parameter, λ, was constrained to be $\lambda \leq 1$)

Sample Shorthand Notation (Gas(A=Ar; N=N_2; H=H_2) Temp(K)_P(mbar) P/P_{GO}))	Fitted Rate Constant k (s^{-1})	Other Fitted Parameter λ; (λ required to be <1)
N77_23 0.8	2.85×10^{-6}	1.00
N77_43 1.4	2.68×10^{-6}	1.00
N77_220 1.6	4.55×10^{-6}	1.00
N77_91 3.0	6.10×10^{-6}	1.00
A77_92	9.74×10^{-6}	1.00
N77_223 7.4	1.99×10^{-5}	1.00
N77_355 12	2.10×10^{-5}	1.00
N87_30 0.3	1.02×10^{-5}	0.917
N87_106 1.0	1.22×10^{-5}	0.947
N87_265 2.4	3.61×10^{-5}	1.00
N87_414 2.5	3.74×10^{-5}	1.00
N87_414 3.8	6.49×10^{-5}	1.00
N87_829 5.0	1.12×10^{-4}	1.00
A87_115 0.2	7.24×10^{-5}	1.00
H87_106	3.92×10^{-4}	0.584

(H) MPD

Sample Shorthand Notation (Gas(A=Ar; N=N_2; H=H_2) Temp(K)_P(mbar) $P/P_{GO)}$)	Fitted Rate Constant k (s^{-1})
N77_23 0.8	1.86×10^{-7}
N77_43 1.4	1.46×10^{-7}
N77_220 1.6	2.07×10^{-7}
N77_91 3.0	3.30×10^{-7}
A77_92	4.26×10^{-7}
N77_223 7.4	1.10×10^{-6}
N77_355 12	1.25×10^{-6}
N87_30 0.3	5.27×10^{-7}
N87_106 1.0	5.91×10^{-7}
N87_265 2.4	1.90×10^{-6}
N87_414 2.5	2.03×10^{-6}
N87_414 3.8	3.56×10^{-6}
N87_829 5.0	5.65×10^{-6}
A87_115 0.2	3.83×10^{-6}
H87_106	2.05×10^{-5}

Table S4: Kinetic parameters of models with best fitting (from **Table S2-S3**).

Sample Shorthand Notation (Gas(A=Ar; $N=N_2$; $H=H_2$) Temp(K)_P(mbar) P/P_{GO}))	Model	Fitted Rate Constants (s^{-1})	Other Fitted Parameters	R^2	AIC
N77_23 0.8	CE	$k = 2.40\times10^{-6}$	$\lambda = 2.24$	0.9976	-7974
N77_43 1.4	CE	$k = 2.67\times10^{-6}$	$\lambda = 1.58$	0.9987	-12537
N77_220 1.6	Gompertz	$k = 1.16 \times 10^{-5}$ $\beta = 5.15 \times 10^{-5}$	-	0.9998	-269
N77_91 3.0	CE	$k = 6.11\times10^{-6}$	$\lambda = 1.59$	0.9997	-8405
A77_92	CE	$k = 8.07\times10^{-6}$	$\lambda = 1.86$	0.9996	-489
N77_223 7.4	PD	$k_{GO} = 3.15\times10^{-5}$ $k_{d1} = 2.50\times10^{-5}$ $k_{d2} = 8.12\times10^{-6}$		0.9999	-23268
N77_355 12	CE	$k = 2.03\times10^{-5}$	$\lambda = 1.51$	0.9999	-9858
N87_30 0.3	PD	$k_{GO} = 4.35\times10^{-5}$ $k_{d1} = 9.92\times10^{-6}$ $k_{d2} = 1.69\times10^{-5}$	-	0.9994	-7482
N87_106 1.0	PD	$k_{GO} = 5.24\times10^{-5}$ $k_{d1} = 1.21\times10^{-5}$ $k_{d2} = 1.65\times10^{-5}$	-	0.9998	-18320
N87_265 2.4	PD	$k_{GO} = 8.98\times10^{-5}$ $k_{d1} = 4.06\times10^{-5}$ $k_{d2} = 1.35\times10^{-5}$	-	1.0000	-34058
N87_414 2.5	PD	$k_{GO} = 3.46\times10^{-5}$ $k_{d1} = 1.42\times10^{-4}$ $k_{d2} = 5.98\times10^{-6}$	-	0.9999	-319
N87_414 3.8	PD	$k_{GO} = 1.79\times10^{-4}$ $k_{d1} = 7.31\times10^{-5}$ $k_{d2} = 1.31\times10^{-5}$	-	1.0000	-29882
N87_829 5.0	PD	$k_{GO} = 3.59\times10^{-4}$ $k_{d1} = 1.24\times10^{-4}$ $k_{d2} = 3.78\times10^{-5}$	-	0.9999	-267
A87_115 0.2	PD	$k_{GO} = 3.96\times10^{-5}$ $k_{d1} = 2.37\times10^{-4}$ $k_{d2} = 3.81\times10^{-5}$	-	1.0000	-51316
H87_106	DE	$k_1 = 1.41\times10^{-4}$ $k_2 = 1.77\times10^{-3}$	$A_1=A_2=0.5$	0.9984	-471

V. Additional Sigmoidal Adsorption Rate Data/Fits to Flexible MOFs from the Literature

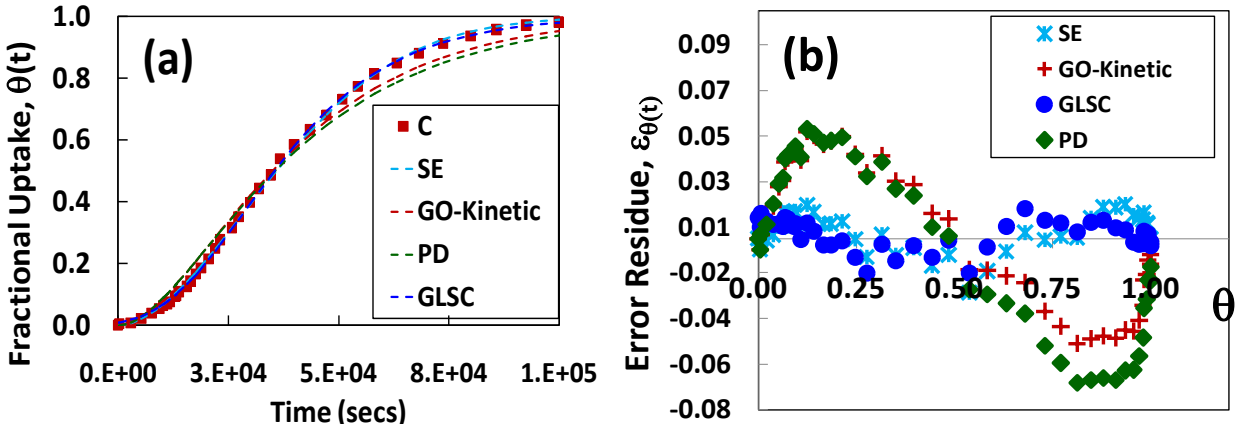

Figure S12: (a) Fits of SE, PD, GO-Kinetic and Gompertz models to data set Cd(bpndc)(bpy) (N_2, 90 K data from[5]) and (b) Error residues (fit-experimental values) for the corresponding fits.

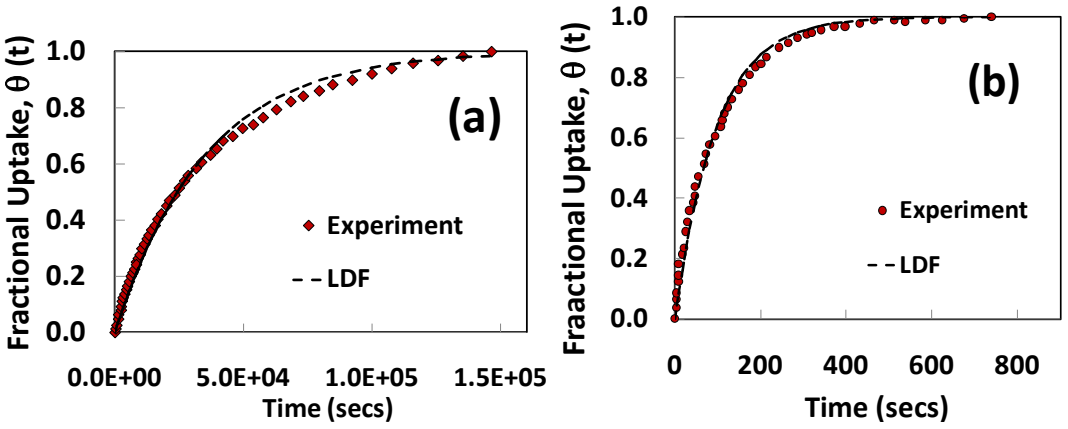

Figure S13: Fits of LDF model to rate data for **(a)** Ar and **(b)** O_2 to Cd(bpndc)(bpy)]n at 90 K from Ref. [5].

Table S5: Fits of rate data at 90 K to kinetic models for adsorption in Cd(bpndc)(bpy)[5]

Gas	Model	Fitted Rate Constants (s^{-1})	Other Fitted Parameters*	R^2
N_2	MPD	$k = 6.7 \times 10^{-5}$	#	0.9541
	LDF	$k = 2 \times 10^{-5}$	#	0.9869
	DE	$k_1 \sim k_2 = 4.5 \times 10^{-6}$	$A_1=A_2=0.5$	0.9802
	SE	$k = 2.3 \times 10^{-5}$	$\lambda=1.83$	0.9997
	GO-Kinetic	$k_{go} \sim k_{d1} \sim k_{d2} = 4.8 \times 10^{-5}$	$A_1=A_2=0.5$	0.9986
	PD	$k_{go}=3.5 \times 10^{-5}$, $k_1=4.8 \times 10^{-5}$, $k_2=1 \times 10^{-7}$	#	0.9981
	Gompertz	$k=5.4 \times 10^{-5}$ and $\beta=2.5 \times 10^{-4}$	$\alpha=4.7$	0.9998
Ar	MPD	$k=1.4 \times 10^{-6}$	#	0.9965
	LDF	$k=2.9 \times 10^{-5}$	#	0.9970
	SE	$k=2.8 \times 10^{-5}$	$\lambda=0.88$	0.9996
	GO-Kinetic	$k_{go}=2 \times 10^{-1}$, $k_{d1}=1.7 \times 10^{-5}$, $k_{d2}=5 \times 10^{-5}$	$A_1=A_2=0.5$	0.9989
	Gompertz	$k=4.1 \times 10^{-5}$ and $\beta=8.6 \times 10^{-5}$	$\alpha=2.1$	0.9770
O_2	MPD	$k=5.6 \times 10^{-4}$	#	0.9963
	LDF	$k=1.04 \times 10^{-2}$	#	0.9975
	SE	$k=1.04 \times 10^{-2}$	$\lambda=0.84$	0.9986
	GO-Kinetic	$k_{go}=3 \times 10^{-2}$, $k_{d1}=0.9$, $k_{d2}=7 \times 10^{-3}$	$A_1=A_2=0.5$	0.9974
	Gompertz	$k=1.4 \times 10^{-2}$ and $\beta=2.8 \times 10^{-2}$	$\alpha=2$	0.9899

VI. Exploration of Catalysis Models

The unreacted core model (UCM) treats fast diffusion and slow reaction, leading to a retreating interface, as shown in Figure S2(i). In the GO process, we consider diffusion of the adsorbate species to the interface at which the phase transition occurs and treat the phase transition as the reaction. Incorporating the pseudo-steady state approximation (PSSA) allows us to decouple the slow reaction at the interface from the fast diffusion to the interface. Assuming reaction can be separated from diffusion and the reaction is first order, leads to a first order decay of the inner core:

$$\Phi = \frac{R_1(t)}{R_2} = e^{-kt} \qquad \text{(SVI-9)}$$

Where R_1 and R_2 are the radius of the retreating interface and total particle, respectively, k is the reaction rate, and t is time. The cumulative uptake in the particle (q) is equal to the flux at the surface of the particle multiplied by the outer particle surface area:

$$q = -\int_0^t 4\pi R_2 D(r)\left(\frac{\partial C(r,t)}{\partial r}\right)_{r=R_2} dt \qquad \text{(SVI-10)}$$

Where $D(r)$ is the diffusion coefficient, and C is the concentration of the species at a given location and time. An alternate expression for the two-regime case in Figure S2 is the sum of the concentration in the outer [blue] annulus plus the flux into the inner [white] annulus:

$$q = 4\pi \int_{R_1}^{R_2} r^2 C_B dr - \int_0^t \left[\left(4\pi r^2\right) D\left(\frac{\partial C}{\partial r}\right)\right]_{r=R_1} dt$$
$$q = 4\pi \int_{R_1}^{R_2} r^2 C_B dr + Q(t) \qquad \text{(SVI-11)}$$

Where *Q(t)* is the cumulative flux up to time *t* into the inner unreacted core. In the limiting case of the UCM in which diffusion in the outer annulus is very fast, the concentration in the outer annulus approaches a constant, C_B:

$$q = \frac{4}{3} C_B \pi \left[R_2^3 - R_1^3 \right] + Q(t) \qquad \text{(SVI-12)}$$

Plugging in (9):

$$q = \frac{4}{3} C_B \pi R_2^3 \left[1 - e^{-kt} \right] + Q(t) \qquad \text{(SVI-13)}$$

The flux into the inner unreacted core, if non-negligible, can be solved using Fick's Second Law. Assuming *D* is a constant in the inner region, and the interfacial concentration is C_B:

$$\frac{\partial C}{\partial t} = \frac{1}{r^2} \frac{\partial}{\partial r} \left(r^2 D \frac{\partial C}{\partial r} \right)$$

$$\frac{\partial C}{\partial t} = D \frac{1}{r^2} \left[r^2 \frac{\partial^2 C}{\partial r^2} + 2r \frac{\partial C}{\partial r} \right]$$

$$\frac{\partial C}{\partial t} = D \left[\frac{\partial^2 C}{\partial r^2} + \frac{2}{r} \frac{\partial C}{\partial r} \right]$$

Let u = Cr

$$\frac{\partial u}{\partial t} = D \left[\frac{\partial^2 u}{\partial r^2} \right]$$

Assuming that the variables are separable: u = g(t) * h(r)

$$\frac{\partial g(t)h(r)}{\partial t} = D \left[\frac{\partial^2 g(t)[h(r)]}{\partial r^2} \right]$$

$$h(r) \frac{\partial g(t)}{\partial t} = D g(t) \left[\frac{\partial^2 h(r)}{\partial r^2} \right]$$

$$\frac{1}{Dg(t)} \frac{\partial g(t)}{\partial t} = \frac{1}{h(r)} \left[\frac{\partial^2 h(r)}{\partial r^2} \right] = -\lambda^2$$

Which ultimately leads to:

$$Q = \frac{(C_B - C_o)R_1^2}{4}\left(1 - \frac{8}{\pi^2}\sum_1^\infty \frac{1}{n^2}\exp\left[-D\frac{n^2\pi^2 t}{R_1^2}\right]\right) \approx \frac{C_B R_1^2}{4}\left(1 - \frac{8}{\pi^2}\sum_1^\infty \frac{1}{n^2}\exp\left[-k_c t\right]\right) \qquad \text{(SVI-14)}$$

Where C_o is the concentration at the center of the particle, and at short time, Co→0.

Alternatively, *Q(t)* can be approximated by the LDF model, which leads to the same mathematical behavior as (14), but with much simpler mathematics:

$$Q = aC_B\left(1 - \exp\left[-k_c t\right]\right) \qquad \text{(SVI-15)}$$

Where k_c is the mass transfer coefficient in the inner core:

$$\frac{Dn^2\pi^2}{R_1^2} = k_c \qquad \text{(SVI-16)}$$

The LDF expression for *Q(t)* leads to:

$$q = \frac{4}{3}C_B\pi R_2^3\left[1 - e^{-kt}\right] + aC_B\left[1 - e^{-k_c t}\right]$$
$$q = \alpha\left[1 - e^{-kt}\right] + \beta\left[1 - e^{-k_c t}\right] \qquad \text{(SVI-17)}$$

The final expression is mathematically identical to the DE model and does not lead to the desired linear behavior for *lnln(θ)* vs *t*. Perhaps notably, if diffusion into the outer core is negligible (as is commonly assumed in the UCM development), *Q→0*, and Equation (SVI-17) reduces simply to the LDF model. Neither the LDF or DE model is capable of reproducing sigmoidal behavior. More detailed treatments were also considered,[6] but could not produce sigmoidal rate curves. We do not consider the PCM consideration here, as it is similar to the Avrami treatment, but the Avrami treatment also takes into account more complex geometrical considerations arising from phase impingement.

VII. Avrami-Type Analysis of the Rate Data

Avrami's analysis considered the kinetics of phase transition from a metastable state, considering temperature (or analogously, pressure or concentration) to be the parameter perturbed beyond the equilibrium condition.[7] However, gradients in the perturbation variable were not specifically considered, and thus diffusion limitations within the particle may influence interpretation of the Avrami exponent, although the basic premise remains valid. Despite this caveat, it is interesting to note the 77 K adsorption rate data meet several of the criteria defined by Avrami for the isokinetic regime. The isokinetic regime is defined by near constant behavior in the ratio of the growth rate to the probability for growth activation with temperature. In this 'isokinetic' regime the following behavior are expected: (1) plots of the fractional transformation versus log time will give rise to parallel curves, and (2) normalization of the amount transformed by a characteristic time (e.g. the time require for 50% transformation) should give rise to a universal curve. The data is plotted in this manner in Figures S14-S15, for 77 and 87 K, respectively. We note the 77K data do meet several of these criteria, and particular groupings of the 87 K data also meet these criteria. However, this is ultimately a test for isokinetic behavior rather, rather than of applicability of Avrami's development. The findings are interesting, but not incredibly conclusive to demonstrate the Avrami treatment is valid.

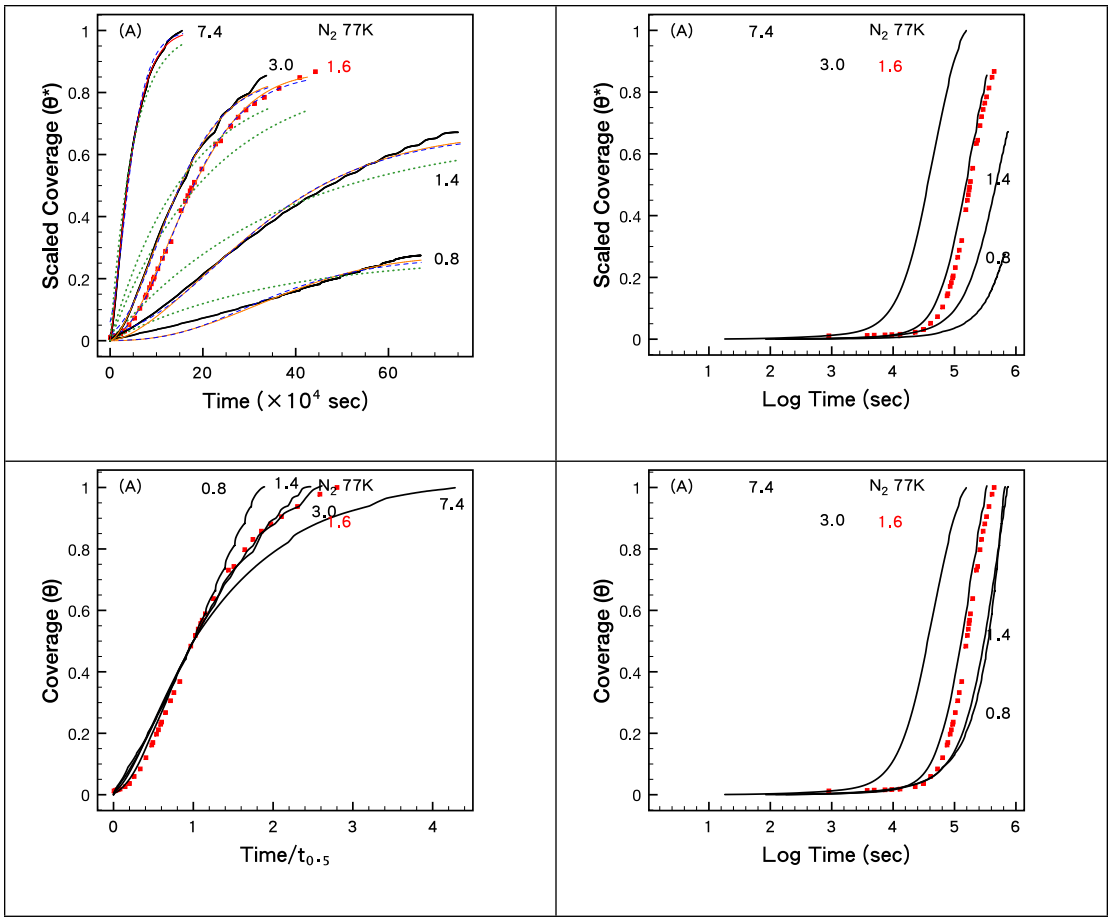

Figure S14: Various tests for isokinetic Avrami-type behavior for the N_2 77 K adsorption data.

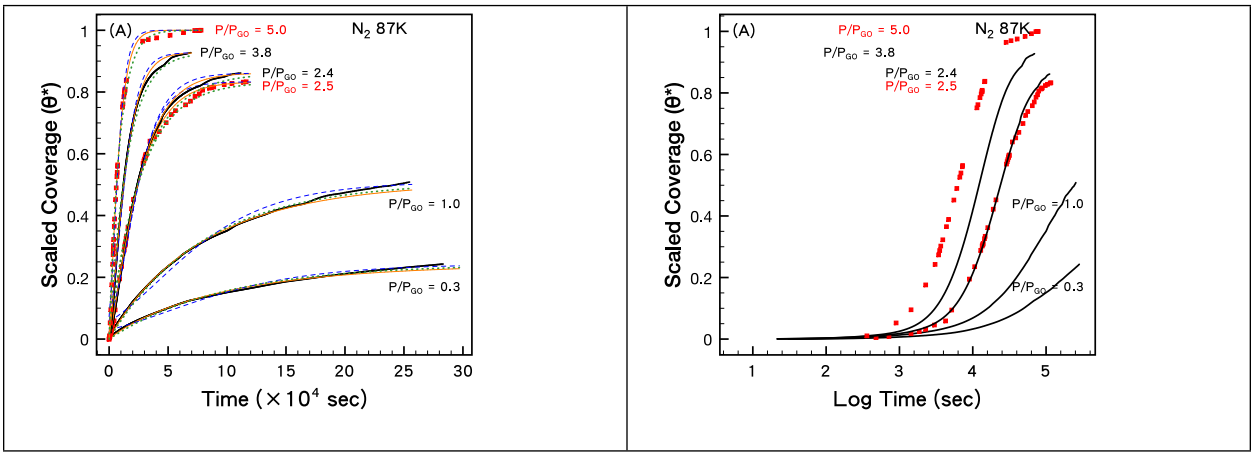

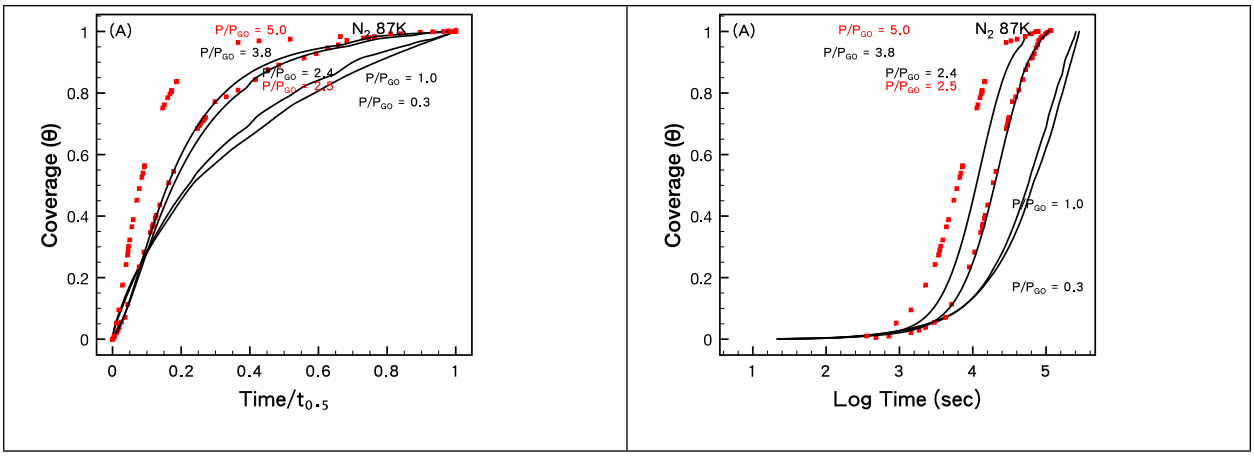

Figure S15: Various tests for isokinetic Avrami-type behavior for the N_2 87 K adsorption data.

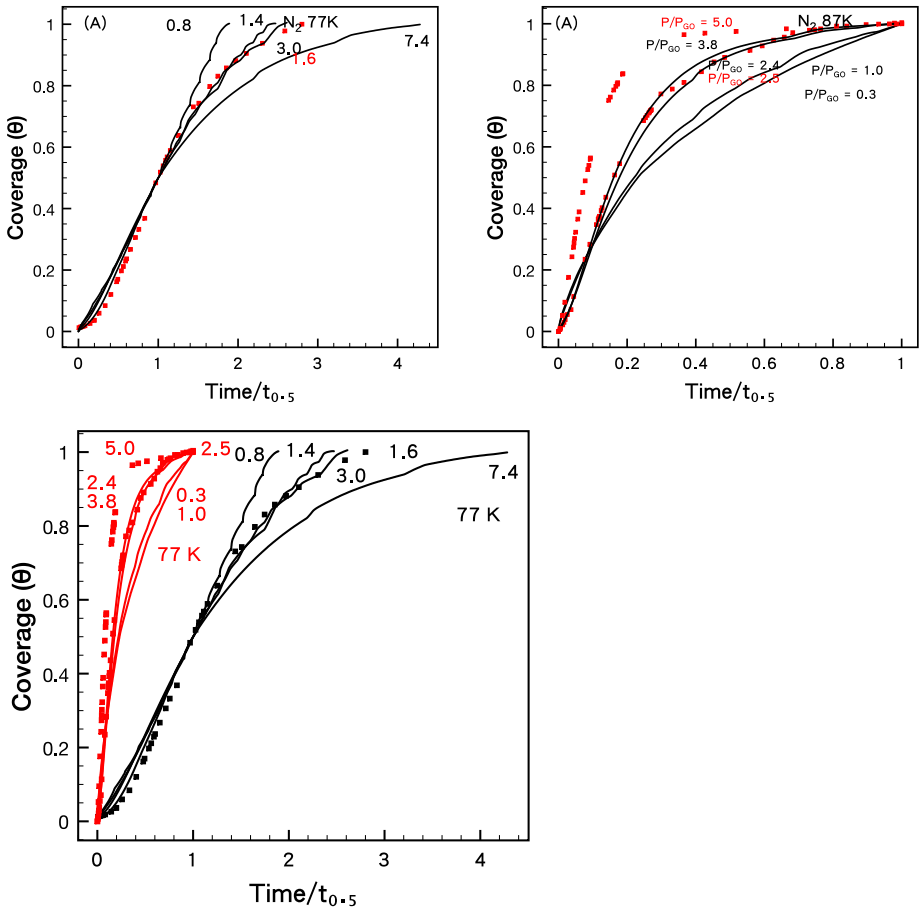

Figure S16: Normalization of data by the characteristic time. (Reproduced from Figures S14 and S15, then merged).

References Cited in the Supporting Information

1. Jain, P.; Fonseca, D. A.; Schaible, E.; Lueking, A. D. Hydrogen uptake of platinum-doped graphite nanoribers and stochastic analysis of hydrogen spillover. *J. Phys. Chem. C* **2007,** *111*, 1788-1800.
2. Li, L.; Bell, J. G.; Tang, S.; Lv, X.; Wang, C.; Xing, Y.; Zhao, X.; Thomas, K. M. Gas Storage and Diffusion through Nanocages and Windows in Porous Metal–Organic Framework Cu2(2,3,5,6-tetramethylbenzene-1,4-diisophthalate)(H2O)2. *Chem Mater* **2014,** *26*, 4679-4695.
3. Cussler, E. L., *Diffusion Mass Transfer in Fluid Systems;* Cambridge University Press: New York, 1997.
4. Christian, J. W., *The Theory of Transformations in Metals and Alloys. Part I: Equilibrium and General Kinetic Theory;* Pergamon Press: Oxford, 1975.
5. Tanaka, D.; Nakagawa, K.; Higuchi, M.; Horike, S.; Kubota, Y.; Kobayashi, L. C.; Takata, M.; Kitagawa, S. Kinetic gate-opening process in a flexible porous coordination polymer. *Angew. Chem. Int. Edit.* **2008,** *47*, 3914-3918.
6. Sircar, S.; Lueking, A. D., Studies of gas adsorption in flexible metal-organic frameworks. In *Gas adsorption in flexible metal-organic frameworks*, Pennsylvania State University: University Park, Pa., 2014.
7. Avrami, M. Kinetics of phase change I - General theory. *J. Chem. Phys.* **1939,** *7*, 1103-1112.